An immutable array of TiO_2 nanotubes to pressures over 30 GPa

2017 Nanotechnology 28 145705

(http://iopscience.iop.org/0957-4484/28/14/145705)

IOP Publishing Nanotechnology
Nanotechnology 28 (2017) 145705 (7pp) https://doi.org/10.1088/1361-6528/aa60fb

An immutable array of TiO_2 nanotubes to pressures over 30 GPa

Yanyan Zhang[1], Qinglin Wang[1,2], Junkai Zhang[1], Xiaoxin Wu[1] and Yanzhang Ma[1,3]

[1] Center for High Pressure Science and Technology Advanced Research, Changchun, 130012, People's Republic of China
[2] Shandong Key Lab of Optical Communication Science and Technology, School of Physical Science & Information Technology of Liaocheng University, Liaocheng, 252059, People's Republic of China
[3] Department of Mechanical Engineering, Texas Technology University, Lubbock, TX 79409, United States of America

E-mail: y.ma@ttu.edu

Received 24 November 2016, revised 3 February 2017
Accepted for publication 16 February 2017
Published 10 March 2017

Abstract

We report the successful formation of an immutable array of α-PbO_2 phase TiO_2 nanotubes by compression of a TiO_2 nanotube array in an anatase phase. During compression to 31.3 GPa, the TiO_2 nanotubes started to directly transform from an anatase phase to a baddeleyite phase at 14.5 GPa and completed the transition at 30.1 GPa. Under decompression, the baddeleyite phase transformed to an α-PbO_2 phase at 4.6 GPa, which was quenchable to ambient pressure. Notably the tubular array microstructure was retained after the application of ultra high pressure and undergoing a series of phase transformations. Measurements indicated that the nanotubes in the array possessed higher compressibility than in the bulk form. The highly aligned array structure is believed to reinforce the nanotubes themselves, giving exceptional stability. This, as well as the wall thickness, may also account for their different phase transition pathway.

Keywords: TiO_2, nanotube arrays, high pressure

(Some figures may appear in colour only in the online journal)

1. Introduction

Since the synthesis of carbon nanotubes in 1991 [1], efforts have focused on the preparation of solid material nano-scale tubular structures such as silica, boron nitride, gallium nitride, TiO_2, and V_2O_5 [2–8]. In the nanotube family, arrayed anodized TiO_2 nanotubes present significant advantages for applications in nano-devices, due to their oriented self-assembly on a substrate [9–14]. The anodized TiO_2 nanotube arrays are amorphous, which can transform to anatase and rutile phases through annealing at elevated temperatures [15]. However, the crystals in TiO_2 nanotubes grow quickly at high temperature and the tubular structure destructs above 800 °C. Therefore, a method that can transform TiO_2 nanotube arrays into other phases and maintain the assembled tubular morphology is highly desirable for various nano-device applications.

Pressure is an alternative method that may successfully tune materials' crystal structures and modify their physical and chemical properties. High-pressure studies on TiO_2 materials have so far revealed three crystalline phases in bulk TiO_2: the anatase phase, the α-PbO_2 phase (~2–5 GPa), and the baddeleyite phase (~12–15 GPa) [16–19]. The phase transformation pressures and stability of TiO_2 nanocrystals are size and morphology dependent. When the particle size is larger than 50 nm, they follow the same transition path as a bulk material. At sizes between 10–50 nm, they by pass the α-PbO_2 phase and directly transform to the baddeleyite phase [19, 20]. Compression of TiO_2 nanoparticles that are smaller than 10 nm leads to amorphization from their anatase phase [21–23]. The morphology-dependence of the anatase to baddeleyite phase transition at high pressure has been observed in 1D TiO_2 nanowires [24–26], 2D nanosheets [27] and random

nanotubes [28]. The phase transitions in either bulk or TiO_2 nanomaterials are irreversible. The high-pressure baddeleyite phase transforms to an α-PbO_2 phase after pressure release to ambient conditions. As a high-pressure phase of bulk TiO_2, α-PbO_2 is quenchable under decompression, before it transforms to a baddeleyite phase.

In the energy related applications such as solar cells [12], lithium batteries [29, 30], and photocatalysis [31, 32], TiO_2 is widely used due to its properties of charge separation and electron transport abilities. However, electron mobility in TiO_2 is very low (0.1–4 $cm^2\,V\,s^{-1}$). Other than doping ion into TiO_2 materials to improve its properties, application of high pressure on TiO_2 materials is an effective method to reduce the resistivity [33]. Furthermore, the electrical conductivity of a quenched α-PbO_2 phase of TiO_2 has been enhanced by ~40% in comparison with that of the anatase phase. Thus, the α-PbO_2 phase of TiO_2 has the potential in the energy conversion applications.

TiO_2 nanotube arrays are promising candidates for various applications due to their unique, highly ordered arrangement and nanosized tubular structure. However, studies have only focused on their anatase and rutile phases. Further investigations of new crystalline structures besides these may provide new possibilities for TiO_2 nanotube array applications. Here, we present an investigation of phase transition behaviors in TiO_2 nanotube arrays under compression to over 30 GPa in a diamond anvil cell. Based on the characterization of the morphologies before and after compression, the TiO_2 nanotube arrays were ultra stable when subjected to high pressures over 30 GPa. We also discuss the size and morphology effects on phase transition behaviors and the stability of nanotube arrays at high pressures.

2. Experimental procedures

The sample was prepared using an electrochemical anodization method [13, 14]. A 0.25 mm thick, 99.5% pure titanium (Ti) foil (Alfa Aesar Co.) was used as our starting material and the substrate for the array synthesis. The foil was attached to the anode-working electrode. Another 0.025 mm thick, 99.9% purity platinum foil (Alfa Aesar Co.) was used as a counter-electrode. A solution of 98 vol% ethylene glycol (99.8% purity, JT Baker) with 2 vol% H_2O and an additional 0.25 wt% ammonium fluoride (NH_4F, 96% purity, Alfa Aesar Co.) served as an electrolyte during synthesis. A voltage of 40 V was applied for 2 h by a DC power supply (IT6874A, ITECH Co.) in the anodization process. The TiO_2 nanotube array film grew on the Ti film in the electrolyte solution during the process. The anodized sample was then washed with an ethanol solution and flushed with deionized water. Subsequently, it was annealed in an oven at 450 °C for 2 h to form the anatase phase of TiO_2 [14]. After annealing, the film was mechanically peeled off the Ti substrate for characterization and further experiments.

We compared the morphologies of the samples before and after compression with a JEM-2100F high-resolution transmission electron microscope (TEM) operated at 200 kV.

During high-pressure processing, a symmetric diamond anvil cell with a 400 μm diameter culet size was used to generate pressure. The sample was loaded into the sample chamber; a 120 μm diameter hole drilled in a preindented rhenium gasket. Subsequently, a ruby sphere as a pressure sensor and a mixture of methanol and ethanol with a volume ratio of 4:1 as a pressure transmitting medium (PTM) were also loaded into the sample chamber. *In situ* high-pressure Raman scattering and synchrotron x-ray diffraction (XRD) measurements were carried out during sample compression and decompression. The Raman measurement was performed by a Renishaw inVia Raman spectrometer with a laser wavelength of 532 nm. The *in situ* synchrotron XRD was under taken at the 15U beam line of the Shanghai Synchrotron Radiation Facility. The x-ray wavelength was 0.6199 Å and the beam size was 10.6 × 7.8 μm^2. The recorded 2D diffraction patterns were integrated into 1D profiles with the Fit2D program [34].

3. Results and discussion

Before high-pressure processing, the morphology and crystal structure of the sample were investigated by TEM and high-resolution TEM (HRTEM), as shown in figure 1. The sample had a highly ordered tubular array structure with a length of a few micrometers, tube diameter of ~100 nm and wall thickness of ~20 nm. The interplanar distance of 0.35 nm, which can be assigned to the (101) planes of anatase TiO_2, indicated that the nanotube array had a pristine anatase structure.

Figure 2(a) displays the XRD patterns in the compression process. At the lowest pressure of 1.3 GPa in the experiments, the diffraction peaks were indexed to the (101), (004) and (200) planes of the anatase phase. With increasing pressure, they slightly shifted to higher 2-theta angles, reflecting a reduction of the interplanary distance with compression. Two new peaks at 12.4° and 13.7° appeared at 16.5 GPa, along with the disappearance of the (004) peak of the anatase phase. These peaks were assigned to the ($\bar{1}$11) and (111) peaks of the baddeleyite phase. All peaks of the anatase phase disappeared and the peaks of baddeleyite phase remained at the experiment's highest pressure of 30.1 GPa. Thus, based on these measurements, the transition from the anatase to baddeleyite phase started from 16.5 GPa and completed at 30.1 GPa. Figure 2(b) displays the diffraction spectra during decompression. A regular drift of all peaks to lower angles was observed during pressure reduction until 9.2 GPa. However, when the sample was finally quenched to ambient conditions from 9.2 GPa, only two diffraction peaks could be indexed to the (111) and (110) peaks of the α-PbO_2 phase. Thus, the sample eventually transformed to and maintained the α-PbO_2 phase at ambient pressure.

To verify the observed phase transition sequence of the TiO_2 nanotube arrays from XRD measurements, Raman spectra were applied to characterize the pressure-induced structural phase transition. At ambient conditions, the anatase TiO_2 tetragonal lattice belonged to the space group D_{4h}^{19}(I4/

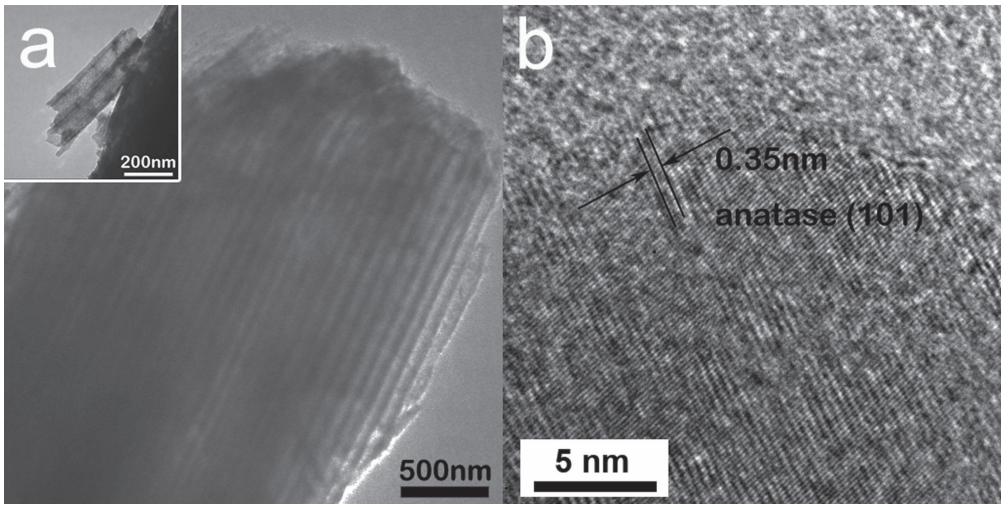

Figure 1. TEM (a) and HRTEM (b) images of the initial sample.

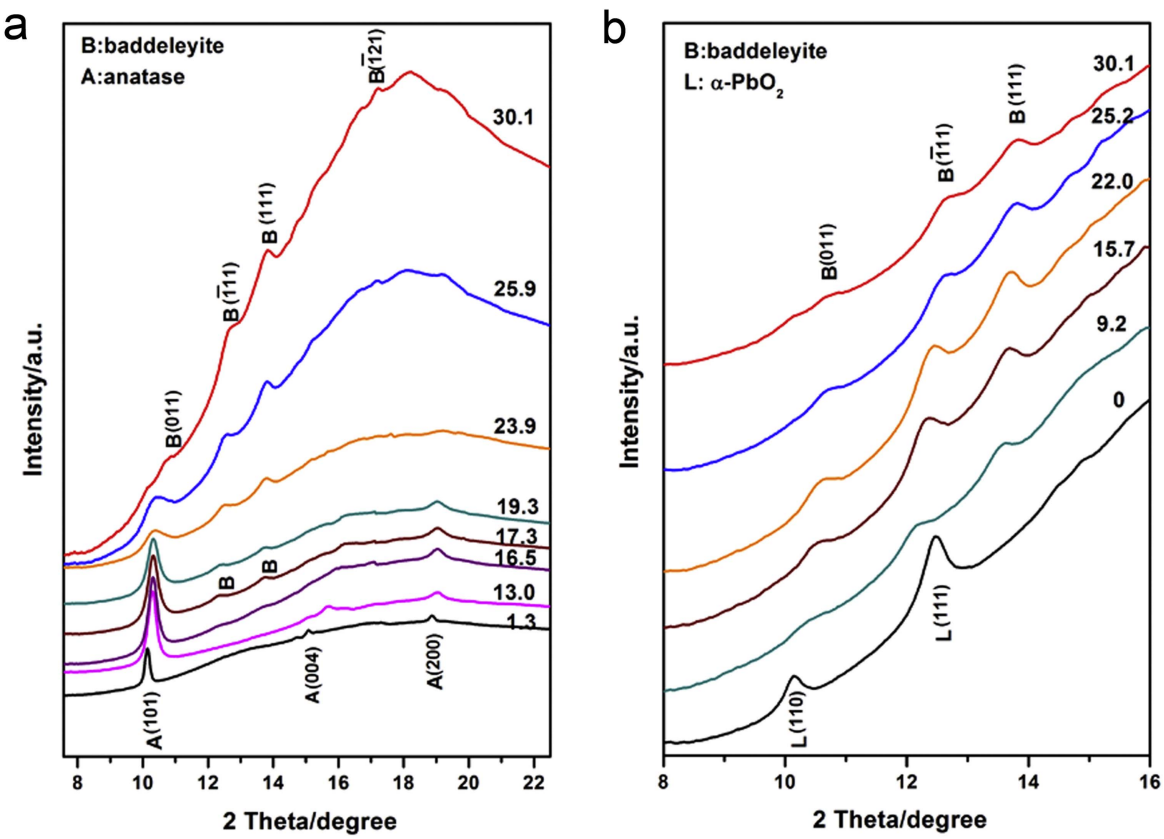

Figure 2. X-ray diffraction patterns of TiO_2 nanotube arrays at selected pressures during: (a) compression and (b) decompression. The pressure in GPa is labeled above each curve.

amd) [35]. According to its primitive unit cell and factor group analysis, it consisted of six Raman modes including the $3E_g$, $2B_{1g}$ and A_{1g} modes. Figure 3 shows the Raman spectra at selected pressures. The spectrum at ambient pressure (the bottom spectrum in figure 3(a)) shows Raman modes at 142, 194, 394, 515 and 635 cm^{-1}, which can be identified as $E_{g(1)}$, $E_{g(2)}$, $B_{1g(1)}$, $A_{1g(1)} + B_{1g(2)}$, and $E_{g(3)}$ [36]. Upon compression, all the Raman modes showed routine blue-shift along with a significant intensity decrease and width increase. A new peak at 489 cm^{-1} was identified from the baddeleyite structure [22, 37] at 14.5 GPa, indicating that a phase transition from the anatase phase to a baddeleyite phase had occurred, which is consistent with our XRD observation. At pressures above 14.5 GPa, this peak grew and another peak from the baddeleyite phase was observed at ~230 cm^{-1} when pressure reached 18.6 GPa. At 31.3 GPa, all the peaks from the anatase phase disappeared and only baddeleyite peaks were visible. It indicated that the anatase phase

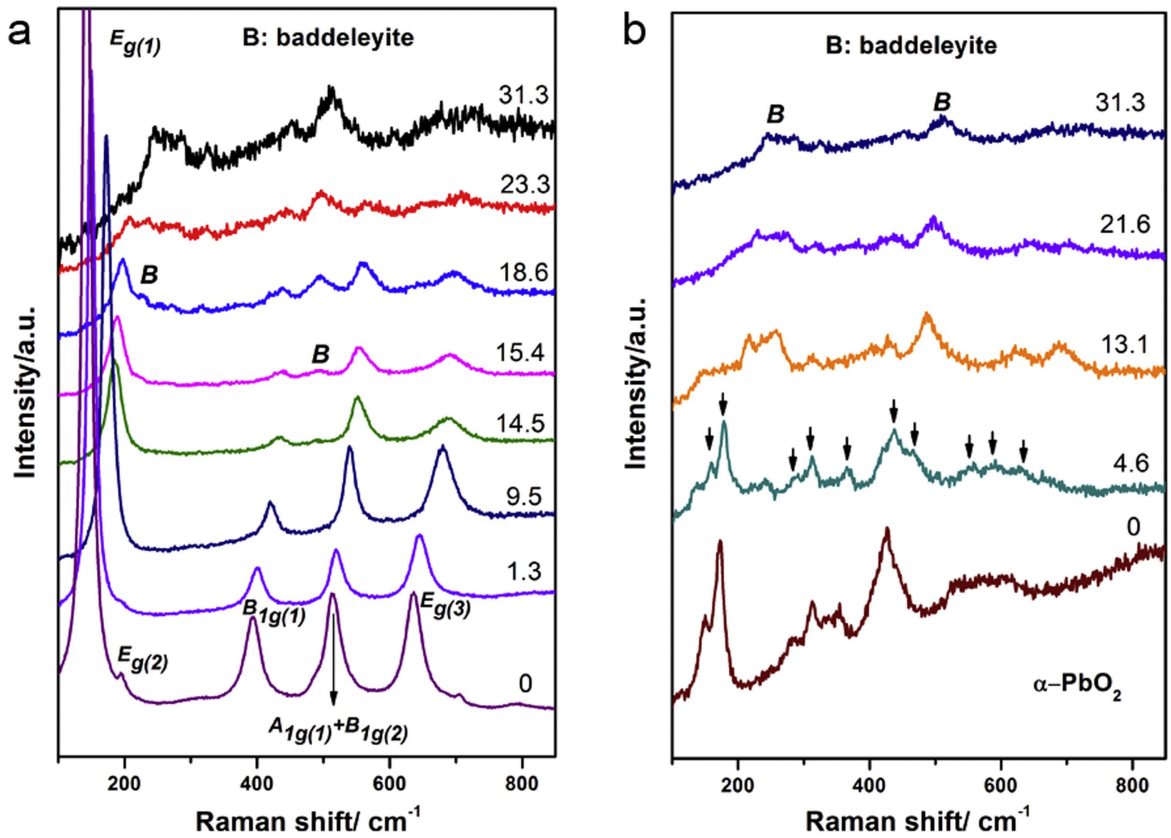

Figure 3. Raman spectra of TiO_2 nanotube arrays during: (a) compression and (b) decompression. The pressure in GPa is labeled above each spectrum.

had completely transformed to the baddeleyite phase. During decompression, all the peaks from the baddeleyite phase remained until 13.1 GPa, as shown in figure 3(b). When pressure decreased to 4.6 GPa, new peaks were observed at 160, 179 , 287, 313, 367, 436, 554, 588, and 632 cm^{-1}. These peaks were all ascribed to scattering from the α-PbO_2 phase. When the sample was finally quenched down to ambient pressure, all the Raman modes from the baddeleyite phase disappeared. The α-PbO_2 phase remained and the intensity of those Raman peaks significantly increased. Thus, we determined that the baddeleyite phase transformed to the α-PbO_2 phase during decompression at 4.6 GPa and the α-PbO_2 phase was quenchable to ambient pressure, which agrees with our XRD results.

To investigate the morphological stability of the TiO_2 nanotube arrays, as well as the crystal structure change, TEM and HRTEM measurements were performed on the quenched sample, as shown in figure 4. The tubular array structure survived after undergoing both compression and decompression (figure 4(a)). Figure 4(b) shows good crystallinity of the quenched TiO_2 nanotube and a clear interplanar distance of 0.28 nm, which is ascribed to the (111) planes of the α-PbO_2 phase. This is consistent with the x-ray and Raman measurement results and demonstrates that the TiO_2 nanotube arrays undergo an anatase to baddeleyite then to α-PbO_2 phase transitions during compression up to ~31 GPa and decompression down to ambient conditions, respectively, without any morphology damage.

The XRD and Raman results clearly suggest that the high-pressure behavior of the anatase structure TiO_2 nanotube arrays differ from the bulk material. It is well known that bulk TiO_2 has a phase transition path from an anatase to an α-PbO_2 phase, and then to a baddeleyite phase during compression. The TiO_2 nanotube arrays present a phase transition sequence similar to some of the nano-sized TiO_2 materials listed in table 1. For the nanoparticles, the phase transition paths are size-dependent. There are two critical sizes (10 and 50 nm) for the anatase TiO_2 particles' transformation to different high-pressure phases. The other TiO_2 materials (nanowires, nanosheets, and random nanotubes) present morphology-dependent phase transitions. Our TiO_2 material has tubular morphology, which allows the PTM to penetrate the tubes and provide a hydrostatic environment for the tube walls. The wall thickness of the tubes is about 20 nm, which is a favorable dimension for the direct phase transition from the anatase phase to the baddeleyite phase. Therefore, we suggest that the unique tubular structure, as well as the nanosized wall thickness, play determining roles in the phase transition behaviors of the TiO_2 nanotube arrays. As shown by our TEM studies, the ultra-stable tubular array structure of this TiO_2 material may also result from its special morphology with a perfectly aligned and compact arrangement. The self-assembled array of TiO_2 nanotubes grew due to the competitive reactions between anodic oxidation and chemical dissolution in the electrolyte [38]. By controlling the fluoride concentration, temperature, anodization potential and reaction

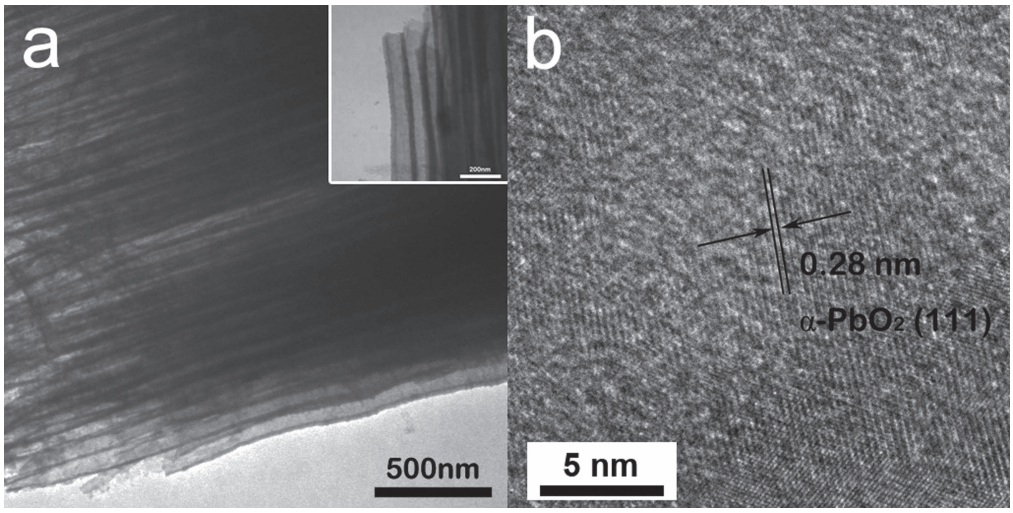

Figure 4. TEM (a) and HRTEM (b) images of TiO_2 nanotubes after release from 31.3 GPa to ambient pressure.

Table 1. Phase transitions in anatase TiO_2 materials with different sizes and morphologies.

Morphologies	Size (nm)	Transition pressure (GPa)	High pressure phases	References
Bulk		2–5	α-PbO_2	[16–19]
		12–15	Baddeleyite	
Nanowires	<200 (diameter)	9–13	Baddeleyite	[25, 26]
Nanoparticles	10–50	11–18	Baddeleyite	[19, 20]
Nanoparticles	<10	~24	Amorphous	[21, 22]
Nanosheets	1:20–40:5–8	14–23	Baddeleyite	[27]
Nanotubes	~5 (diameter)	18	Baddeleyite	[28]
Nanotubes	~20 (wall thickness)	~15	Baddeleyite	This study

time, the tubes finally grew close to each other in an oriented arrangement. The tubular microstructure and compact array bundles effectively reinforced themselves, resisting destruction from ultra-high external pressure and preventing damage of the aligned arrangement. The PTM distribution of the inner and outer nanotubes contributes to balancing the external pressure on the walls and maintaining the tubular morphology.

Figure 5 is the pressure dependence of the *d*-spacings during compression. It is clear that the distances between the (101), (004) and (200) planes of the anatase phase decrease with increasing pressure, but their reduction rate is different. The d-spacing of the (004) plane presented the highest rate of reduction before it disappeared at ~14.0 GPa, while the (200) plane decreased at the lowest rate. These inconsistent rates indicate different compressibility on the *a*- and *c*-axis. From the lattice parameter reduction ratio (a/a_0 and c/c_0) as a function of pressure, the crystal lattice of the TiO_2 nanotube is more compressible along the *c*-axis than the *a*-axis, as shown in figure 6. This phenomenon has also been found in other TiO_2 materials such as bulk [17], nanosheets [27], nanowire [24] and hydrothermal nanotubes [28], as plotted in figure 6. The anatase structure consists of edge-sharing TiO_6 octahedra [39] and the Ti atom-occupied oxygen octahedron is much harder than the soft empty one. Thus, the different directional population of the hard occupied (TiO_6) and soft empty (O_6) oxygen octahedra attribute to the material's different

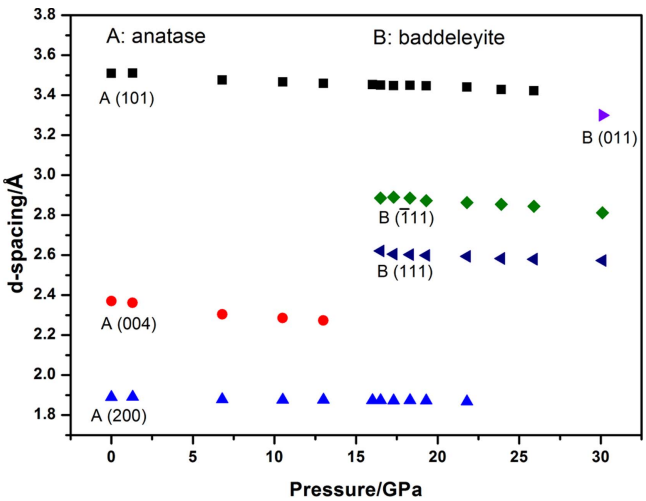

Figure 5. Pressure dependence of the *d*-spacings of nanotube arrays.

compressibility along the *a*-axis and *c*-axis. By comparing the normalized cell parameters of TiO_2 nanotube arrays with other TiO_2 materials, there is no significant *a*-axis compressibility difference between them but the *c*-axis of the TiO_2 nanotube arrays has much higher compressibility. This may cause the nanotube arrays to be more compressible than other TiO_2 materials.

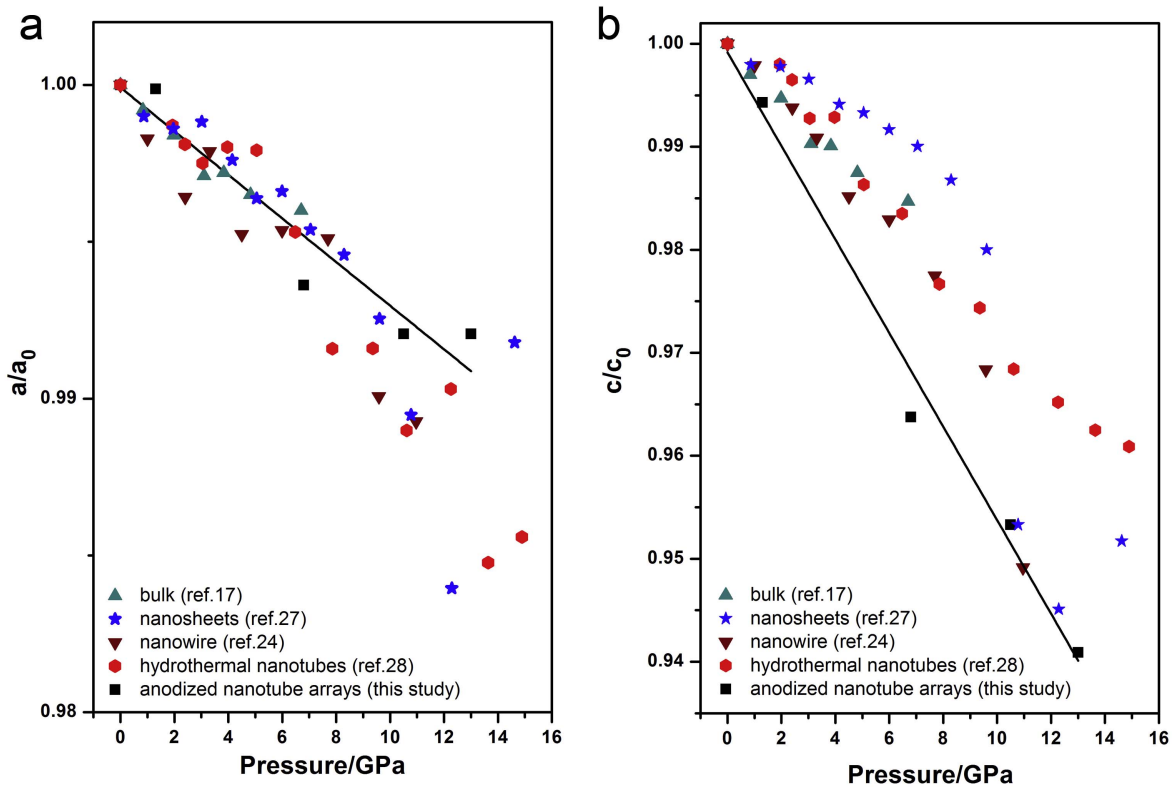

Figure 6. Normalized cell parameters of TiO_2 nanotube arrays at pressures. Solid lines are the linear fitting in this study.

Analysis of the volume reduction as a function of pressure allows further understanding of TiO_2 nanotube array compressibility. This is compared with earlier studies of TiO_2 with various sizes and morphologies in figure 7. The bulk modulus is calculated by fitting the third-order Birch Murnaghan equation:

$$P = 3/2B_0[(V/V_0)^{-7/3} - (V/V_0)^{-5/3}] \times \{1 + 3/4(B_0' - 4)[(V/V_0)^{-2/3} - 1]\},$$

where V is the volume at pressure P, V_0 is the volume at zero-pressure, and B_0 and B_0' are the isothermal bulk modulus and its pressure derivative, respectively. The bulk modulus (B_0) of the nanotube arrays is determined as 140 ± 9 GPa when B_0' is fixed at 4. It is smaller than those (166–317 GPa) of the reported bulk TiO_2 [17] and nano-sized materials [20, 21, 24, 27, 28, 40, 41]. Compared to the compressibility of different morphologies along the a- and c-axes, the slope of c/c_0 from the nanotube arrays was two times that of the bulk. We ascribe this low bulk modulus in the nanotube arrays to the high shrinking rate in the c-axis, which is shown in figure 6.

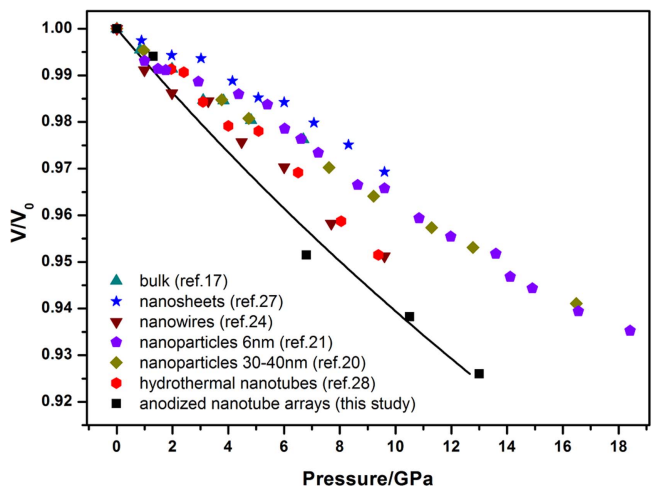

Figure 7. The volume reduction of the anatase phase of TiO_2 nanotube arrays.

4. Conclusions

We studied the behaviors of anatase TiO_2 nanotube arrays at high pressures. Upon compression, the intermediate α-PbO_2 phase was missing, which contrasts with the phase transitions in a bulk TiO_2 material. The anatase phase started transformation to a baddeleyite phase at 14.5 GPa upon compression. The baddeleyite phase transformed to the α-PbO_2 phase during decompression. The 3D TiO_2 nanotubes had ultra-stable morphology and presented very high compressibility under pressure up to 31.3 GPa, which demonstrates that TiO_2 nanotubes with a good crystalline α-PbO_2 phase can be formed by high-pressure processing. These pressure-induced phase transitions in TiO_2 nanotube arrays provide a new candidate to develop α-PbO_2 phase based nano-devices of nanotubes.

Acknowledgements

This work was performed at BL15U1 beam line, Shanghai Synchrotron Radiation Facility (SSRF) in China. The authors would like to thank SSRF for use of the synchrotron radiation facilities.

References

[1] Iijima S 1991 *Nature* **354** 56–8
[2] Martin C R 1994 *Science* **266** 1961–5
[3] Ajayan P M, Stephan O, Redlich P H and Colliex C 1996 *Nature* **375** 564–6
[4] Schmidt O G and Eberl K 2001 *Nature* **410** 168
[5] Pokropivnyi V V 2001 *Powder Metall. Met. Ceram.* **40** 11–2
[6] Hoyer P 1996 *Adv. Mater.* **8** 857–9
[7] Kasuga T, Hiramatsu M, Hoson A, Sekino T and Niihara K 1998 *Langmuir* **14** 3160–3
[8] Krumeich F, Muhr H J, Niedeberger M, Brieri F, Schnyder B and Nesper R 1999 *J. Am. Chem. Soc.* **121** 8324–31
[9] Oh S, Brammer K, Li J, Teng D, Engler A, Chien S and Jin S 2009 *Proc. Natl Acad. Sci.* **106** 2130–5
[10] Oh S, Daraio C, Chen L H, Pisanic T R and Jin S 2006 *J. Biomed. Mater. Res.* **78A** 97–103
[11] Park J H, Kim S and Bard A J 2006 *Nano Lett.* **6** 24–8
[12] Zhang Y, Khamwannah J, Kim H, Noh S Y, Yang H and Jin S 2013 *Nanotechnology* **24** 045401
[13] Ma J, Yang M, Sun Y, Li C, Li Q, Gao F, Yua F and Chen J 2014 *Physica* E **58** 24–9
[14] Zhang Y, Fu W, Yang H, Qi Q, Zeng Y, Zhang T, Ge R and Zou G 2008 *Appl. Surf. Sci.* **254** 5545–7
[15] Zhang Y *et al* 2009 *Thin Solid Films* **518** 99–103
[16] Ohsaka T, Yamaoka S and Shimomura O 1979 *Solid State Commun.* **30** 345–7
[17] Mammone J F, Sharma S K and Nicol M 1980 *Solid State Commun.* **34** 799–802
[18] Dewhurst J K and Lowther J E 1996 *Phys. Rev.* B **54** R3673
[19] Hearne G R, Zhao J, Dawe A M, Pischedda V, Maaza M, Nieuwoudt M K, Kibasomba P, Nemraoui O, Comins J D and Witcomb M J 2004 *Phys. Rev.* B **70** 134102
[20] Swamy V, Kuznetsov A, Dubrovinsky L S, Caruso R A, Shchukin D G and Muddle B C 2005 *Phys. Rev.* B **71** 184302
[21] Pischedda V, Hearne G R, Dawe A M and Lowther J E 2006 *Phys. Rev. Lett.* **96** 035509
[22] Swamy V, Kuznetsov A Y, Dubrovinsky L S, McMillan P F, Prakapenka V B, Shen G and Muddle B C 2006 *Phys. Rev. Lett.* **96** 135702
[23] Swamy V, Kuznetsov A Y, Dubrovinsky L S, Kurnosov A and Prakapenka V B 2009 *Phys. Rev. Lett.* **103** 075505
[24] Li Q, Cheng B, Yang X, Liu R, Liu B, Liu J, Chen Z, Zou B, Cui T and Liu B 2013 *J. Phys. Chem.* C **117** 8516–21
[25] Dong Z and Song Y 2015 *Can. J. Chem.* **93** 165–72
[26] Li Q, Liu B, Wang L, Li D, Liu R, Zou B, Cui T and Zou G 2010 *J. Phys. Chem. Lett.* **1** 309–14
[27] Li Q, Cheng B, Tian B, Liu R, Liu B, Wang F, Chen Z, Zou B, Cui T and Liu B 2014 *RSC Adv.* **4** 12873
[28] Li Q, Liu R, Wang T, Xu K, Dong Q, Liu B, Liu J and Liu B 2015 *AIP Adv.* **5** 097128
[29] Chen J S, Tan Y L, Li C M, Cheah Y L, Luan D, Madhavi S, Boey F Y C, Archer L A and Lou X W 2010 *J. Am. Chem. Soc.* **132** 6124–30
[30] Shen L, Zhang X, Li H, Yuan C and Cao G 2011 *J. Phys. Chem. Lett.* **2** 3096–101
[31] Linsebigler A L, Lu G and Yates J T 1995 *Chem. Rev.* **95** 735–58
[32] Xu C, Yang W, Guo Q, Dai D, Chen M and Yang X 2013 *J. Am. Chem. Soc.* **135** 10206–9
[33] Lü X, Yang W, Quan Z, Lin T, Bai L, Wang L, Huang F and Zhao Y 2014 *J. Am. Chem. Soc.* **136** 419–26
[34] Hammersley A P, Svensson S O, Hanfland M, Fitch A N and Häusermann D 1996 *High Pressure Res.* **14** 235–48
[35] Wyckoff R W G 1965 *Crystal Structures* vol 1 (New York: Interscience Publishers) p 253
[36] Ohsaka T, Izumi F and Fujiki Y 1978 *J. Raman Spectrosc.* **7** 321–4
[37] Flank A M, Lagarde P, Itie J P, Polian A and Hearne G R 2008 *Phys. Rev.* B **77** 224112
[38] Robin A, Ribeiro M B A, Rosa J L, Nakazatoand R Z and Silva M B 2014 *J. Surf. Eng. Mater. Adv. Technol.* **4** 123–30
[39] Park S W, Jang J T, Cheon J, Lee H H, Lee D R and Lee Y 2008 *J. Phys. Chem.* C **112** 9627–31
[40] Swamy V, Dubrovinsky L S, Dubrovinskaia N A, Simionovici A S, Drakopoulos M, Dmitriev V and Weber H 2003 *Solid State Commun.* **125** 111–5
[41] Arlt T, Bermejo M, Blanco M A, Gerward L, Jiang J Z, Olsen J S and Recio J M 2000 *Phys. Rev.* B **61** 14414